Legends

Figure 1. The structures of 2'-deoxyadenosine (A) and 2'-deoxyaristeromycin (B).

Figure 2. Schematic view of the interresidue NOEs from NOESY spectra used in the structure refinements as contraints. Note how both conformations show typical B-DNA type NOE connectivity pattern for the Watson-Crick basepaired residues (C^1-A^5 and T^8-G^{12}). The central Hoogsteen basepaired residues ($\underline{A}^6$-T^7) however are different and most significantly there is a break in H6/8^n-sugar proton^{n-1} contacts between residue A^5 and $\underline{A}^6$, indicating a change in the base stacking in the centre of the duplex.

Figure 3. The distribution of the NMR derived NOE and dihedral constraints over the different residues for the Watson-Crick (**1A**) and Hoogsteen (**1B**) basepaired structures. The Watson-Crick structure (**1A**) showed the following NOEs: 127 intraresidue, 97 interresidue and 34 cross-strand, giving a total of 258 NOE constraints per strand. The Hoogsteen structure (**1B**) showed: 114 intraresidue, 92 interresidue and 30 cross-strand, giving a total of 236 NOE constraints per strand. This gives an average of 22 and 20 NOEs per residue and strand respectively. A total of 55 NMR-derived dihedral constraints per strand were also used to model both structures.

Figure 4. The CD spectra of the modified dodecamer (**1**, dashed line) compared to the natural counterpart (**2**, solid line): 8 µM oligo in 1M NaCl, 200 mM phosphate (pH 7.3) at 20ºC.

Figure 5. Two sets of sequential imino-imino NOEs can be traced at 0°C (panel A) and 20°C (panel B) for [5'-d($C^1G^2C^3G^4A^5\underline{A}^6T^7T^8C^9G^{10}C^{11}G^{12}$)-3']$_2$. The terminal residues (G^2, G^{10}, G^{12}) of the Watson-Crick basepaired set (**1A**, solid lines, plain font) and the Hoogsteen basepaired set (**1B**, dashed lines, *italic* font) have isochronous chemical shifts while the central ones (residue G^4, T^7, T^8) show significant differences in chemical shifts. Note that at 20°C the central imino protons of the two traces show exchange crosspeaks (boxes a, b and c). See our website: http://bioorgchem.boc.uu.se/ for Figures in colour.

Figure 6. NOESY spectra in H_2O at 0ºC showing imino-MeT/amino/H2 crosspeaks. Note the H8A^6-H3T^7 and T^8 (boxes: a and b) and H1'A^6-H3T^7 (box c) typical for Hoogsteen basepairing (solid lines, plain font: Watson-Crick [**1A**], dashed lines, *italic* font: Hoogsteen duplex [**1B**]). See our website: http://bioorgchem.boc.uu.se/ for Figures in colour.

Figure 7. Schematic view of two A-T basepairs showing various key distances amongst imino-amino-aromatic-sugarH1' in a Watson-Crick (A) vis-à-vis a Hoogsteen (B) (*9a,10*) basepair. For the Hoogsteen basepaired structure (B), magnetisation transfer from H3T^7 to H1'A^6 is possible, through both direct dipolar interaction (5.1 Å) and through spin diffusion through H8$\underline{A}^6$. The *syn* conformation across the glycosidic bond of the adenosine nucleotide brings the H3T^7 and H8$\underline{A}^6$ (2.6Å) as well as H8$\underline{A}^6$ and H1'$\underline{A}^6$ (2.6Å) into close proximity of each other. The same crosspeak for the Watson-Crick basepaired structure (A), with both aglycons in *anti* conformations, is however expected to be much weaker (or not observable) under normal conditions because the magnetisation would have to be transferred 6.8 Å through space or by spin diffusion through 4 steps covering a total distance of 13.6Å (3.1 + 1.8 + 4.9 + 3.8 Å).

Figure 8. NOESY spectra of the aroamtic-H1' region at 0°C. Note the strong H8A^6-H1'A^6 NOE (marked with arrow) indicating a *syn* conformation (solid lines, plain font: Watson-Crick [**1A**], dashed lines, *italic* font: Hoogsteen duplex [**1B**]). See our website: http://bioorgchem.boc.uu.se/ for Figures in colour.

Figure 9. NOESY spectra recorded at 0ºC showing two sets of aromatic-aromatic NOEs. The Watson-Crick basepaired duplex (**1A**, solid lines, plain font) shows standard H8/H6 to H8/H6 interactions whereas in the Hoogsteen basepaired duplex (**1B**, dashed lines, *italic* font) there is an interruption between H8A^5 and H8A^6. Instead there is a crosspeak between H8A^5 to H2A^6 showing that there is most likely a flip of the glycosyl torsion, thus bringing them into a close proximity. See our website: http://bioorgchem.boc.uu.se/ for Figures in colour.

Figure 10. (A) Temperature-dependent 1D spectra of the coalescence process of two MeT^7 resonances (coming from the two duplex conformations) into one NMR time average signal. The resonance at 400 Hz belongs to an impurity that shows no temperature-dependent drift. (B) Lineshape simulation (*18*) of the coalescence process of the same two resonances of MeT^7 using the calculated rate constants, k_4 and k_1 (extrapolated at temperatures above 25°C), from the exchange studies, showing that the appearances of the experimental (A) and the simulated (B) spectra are virtually identical. (C) Comparison of the chemical shifts derived from the coalescence simulation (10B) and those of the experimentally acquired 1D spectra (10A). The shifts from the simulation coalesce around 50°C, and the chemical shift of the simulated averaged resonance at high temperature match with that of the experimentally observed signal before the interconverting duplexes melt to the single strand form.

Figure 11. Superimposition of 8 representative Watson-Crick basepaired duplexes (**1A**) [RMSD = 0.49]. The modified residue, A^6, is highlighted in green.

Figure 12. Superimposition of 8 representative Hoogsteen basepaired duplexes (**1B**) in Group 1 [RMSD = 0.46]. The modified residue, A^6, is highlighted in green.

Figure 13. Superimposition of 8 representative Hoogsteen basepaired duplexes (**1B**) in Group 2 [RMSD = 0.45]. The modified residue, A^6, is highlighted in green.

Figure 14. Comparison of the backbone torsions of the final average structures between the natural duplex (**2**) (*4*) and the two duplex structures (**1A** and **1B**) containing 2'-deoxyaristeromycin.

Figure 15. Comparison of some helical parameters of the final average structures between the natural duplex (**2**) (*4*) structure and the two duplex structures (**1A** and **1B**) containing 2'-deoxyaristeromycin (**1**).

Figure 16. Superimposition of the final average structures for the Watson-Crick basepaired duplex (**1A**) (magenta) and the Hoogsteen basepaired duplexes (**1B**) from Groups 1 (yellow) and 2 (cyan). The RMSD between the Watson-Crick structure and the Hoogsteen structures is 1.5-1.7 Å (Table 5).

Figure 17. A zoom of the central basepairs (Watson-Crick: magenta, Hoogsteen group 1: yellow, Hoogsteen group 2: cyan).

Figure 18. Arrhenius plot of the rate constants k_4 and k_1 determined by a combination of ROESY/NOESY experiments at various mixing times and temperatures. The slope gives the energy of activation, E_a, which gives the contributions of enthalpy, $?H^{\circ\ddagger}$, and entropy, $?S^{\circ\ddagger}$, of activation.

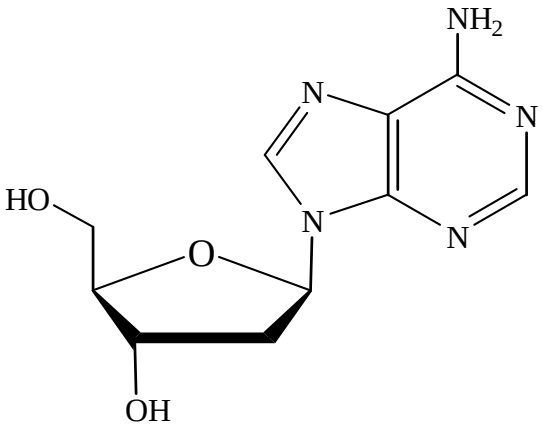

(A)

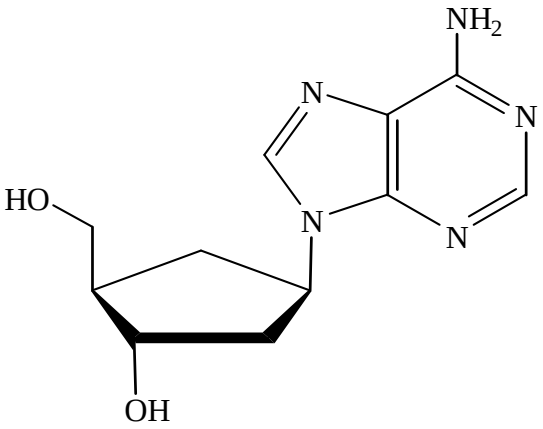

(B)

Figure 1

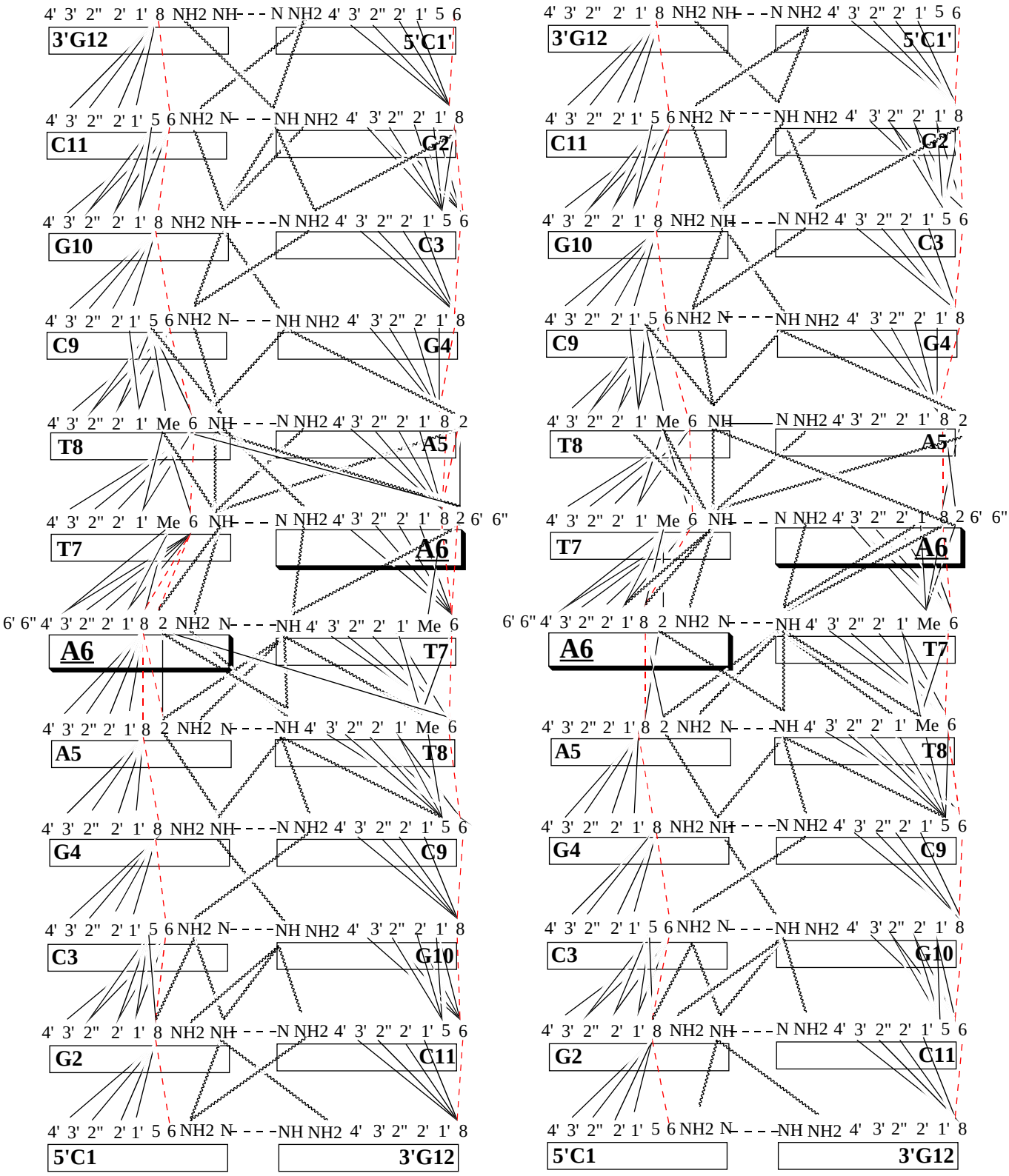
(1A): W-C bp Duplex
(1B): Hoogsteen bp Duplex
3'G12
5'C1'
C11
G2
G10
C3
C9
G4
T8
A5
T7
A6
A6
T7
A5
T8
G4
C9
C3
G10
G2
C11
5'C1
3'G12

Figure 2

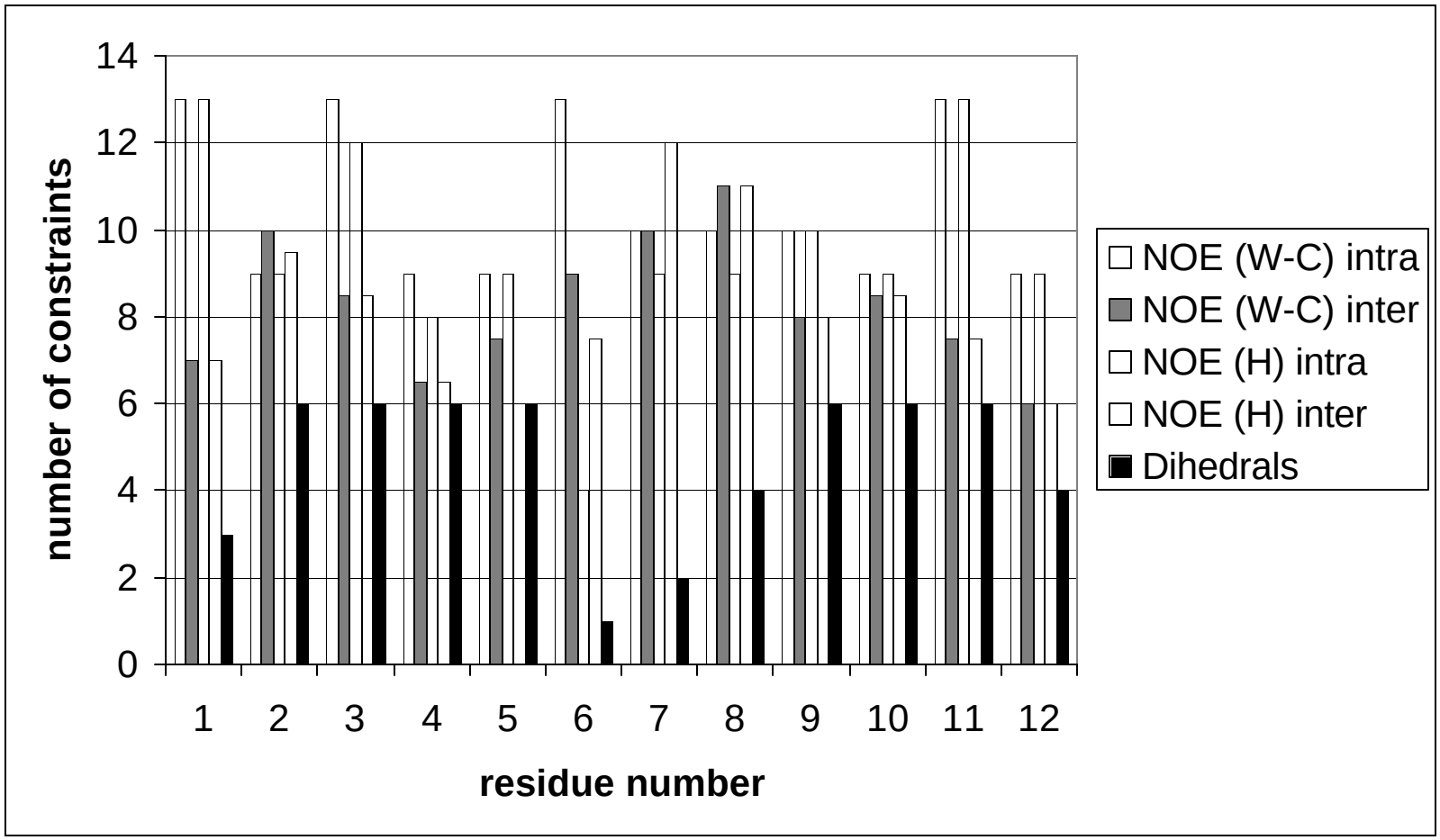
number of constraints
14
12
10
8
6
4
2
0
1
2
3
4
5
6
7
8
9
10
11
12
residue number
NOE (W-C) intra
NOE (W-C) inter
NOE (H) intra
NOE (H) inter
Dihedrals

Figure 3

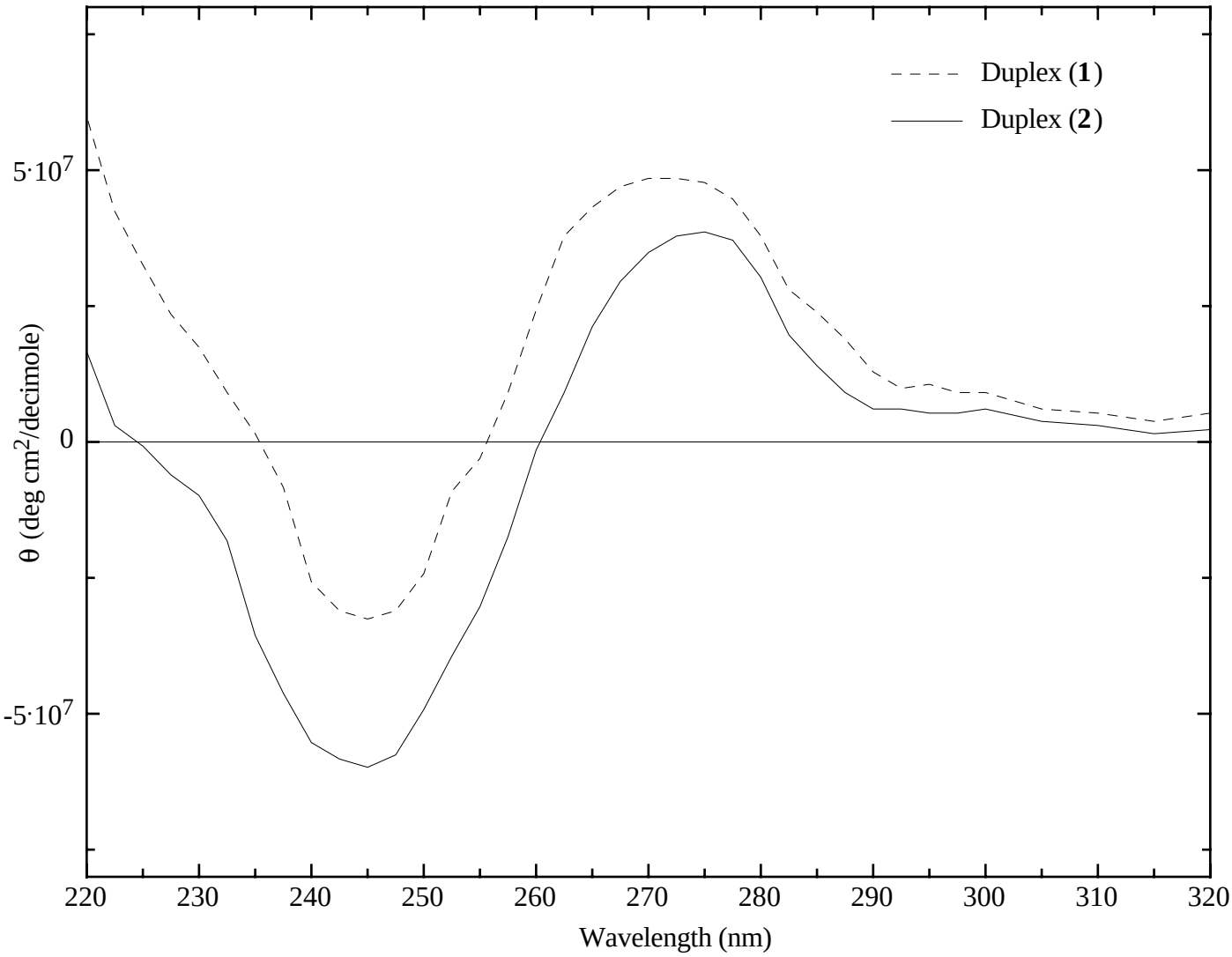
Duplex (1)
Duplex (2)
5·10^7
0
-5·10^7
θ (deg cm^2/decimole)
220
230
240
250
260
270
280
290
300
310
320
Wavelength (nm)

Figure 4

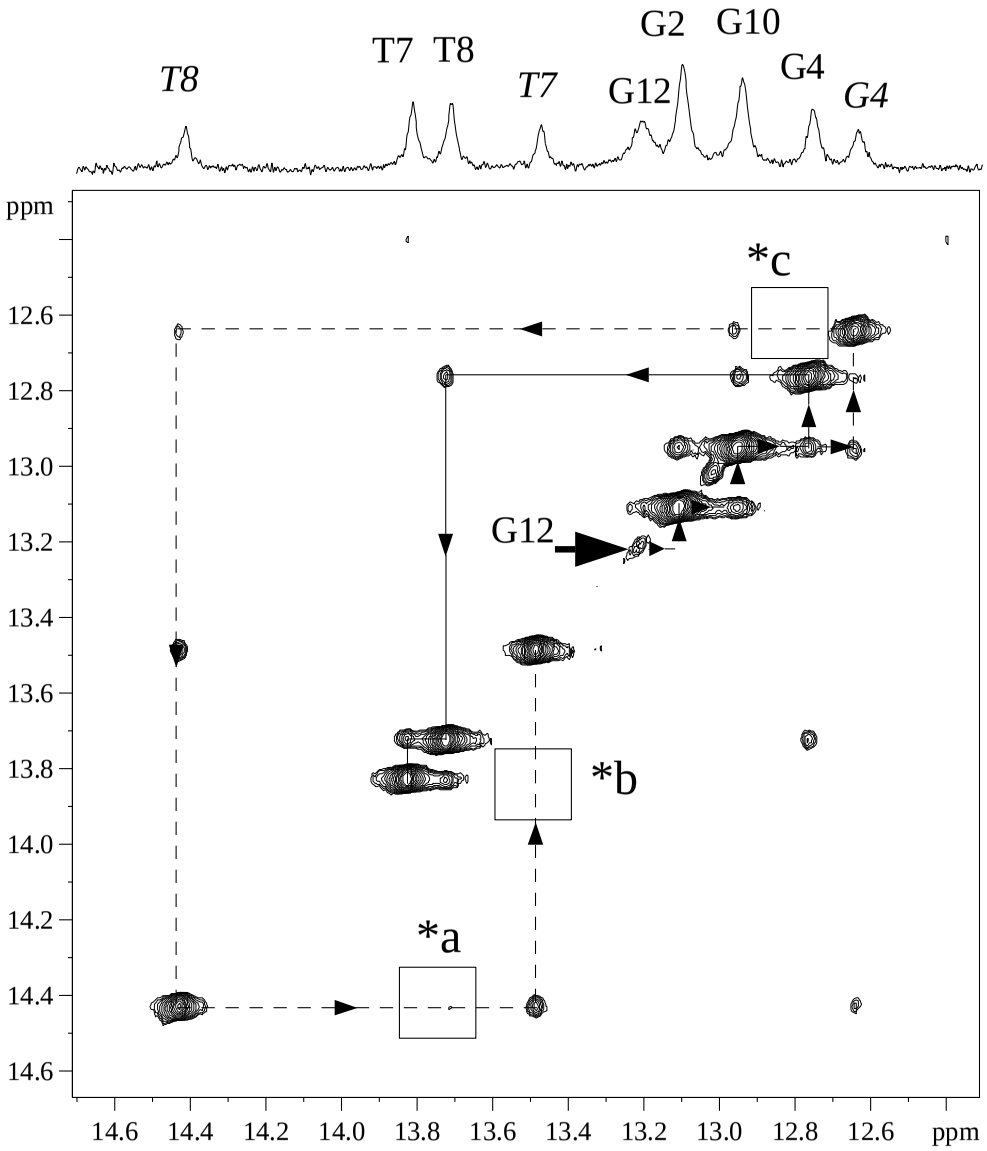
T8
T7 T8
T7
G2
G12
G10
G4
G4
ppm
*c
G12
*b
*a
12.6
12.8
13.0
13.2
13.4
13.6
13.8
14.0
14.2
14.4
14.6
14.6 14.4 14.2 14.0 13.8 13.6 13.4 13.2 13.0 12.8 12.6 ppm

(A)

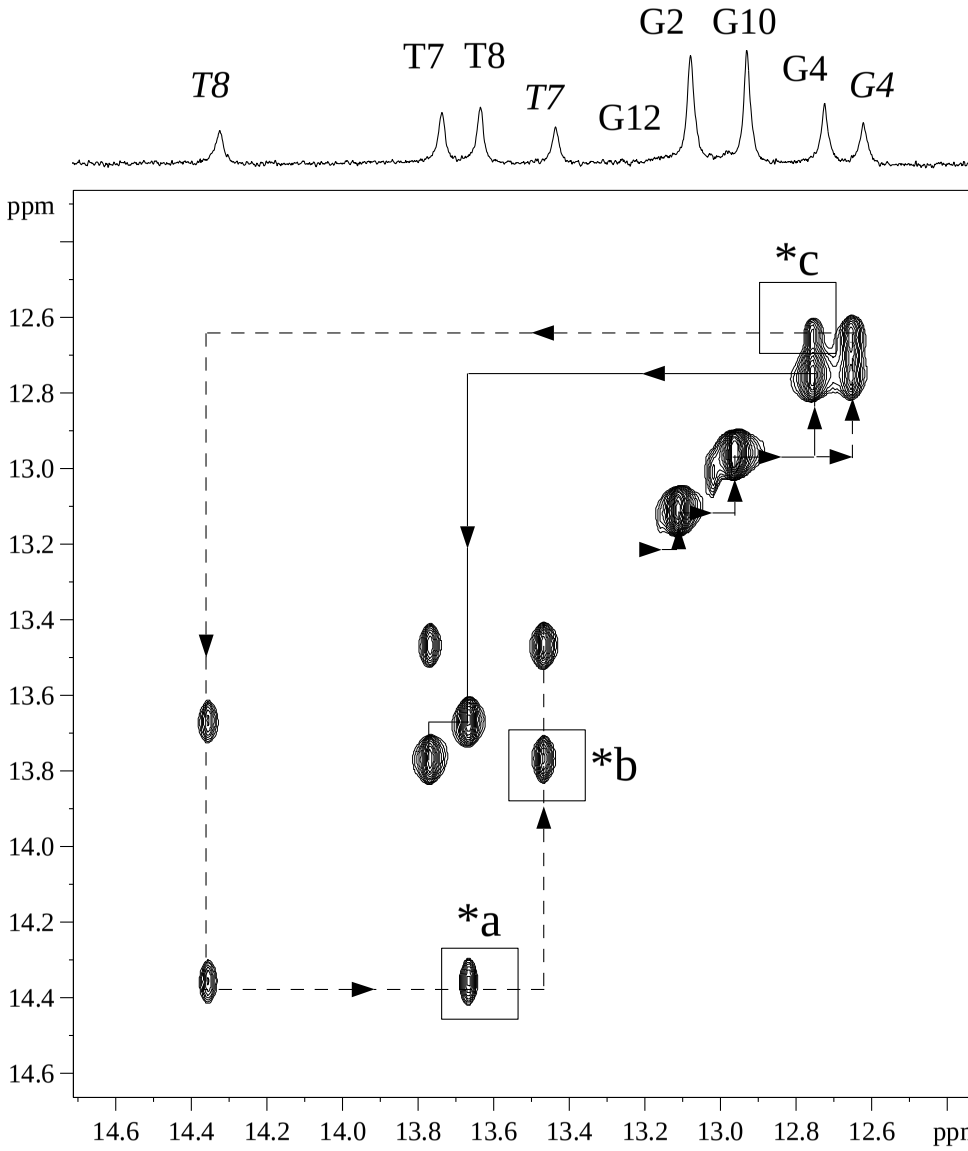
T8
T7 T8
T7
G2
G12
G10
G4
G4
ppm
*c
*b
*a
12.6
12.8
13.0
13.2
13.4
13.6
13.8
14.0
14.2
14.4
14.6
14.6 14.4 14.2 14.0 13.8 13.6 13.4 13.2 13.0 12.8 12.6 ppm

(B)

Figure 5

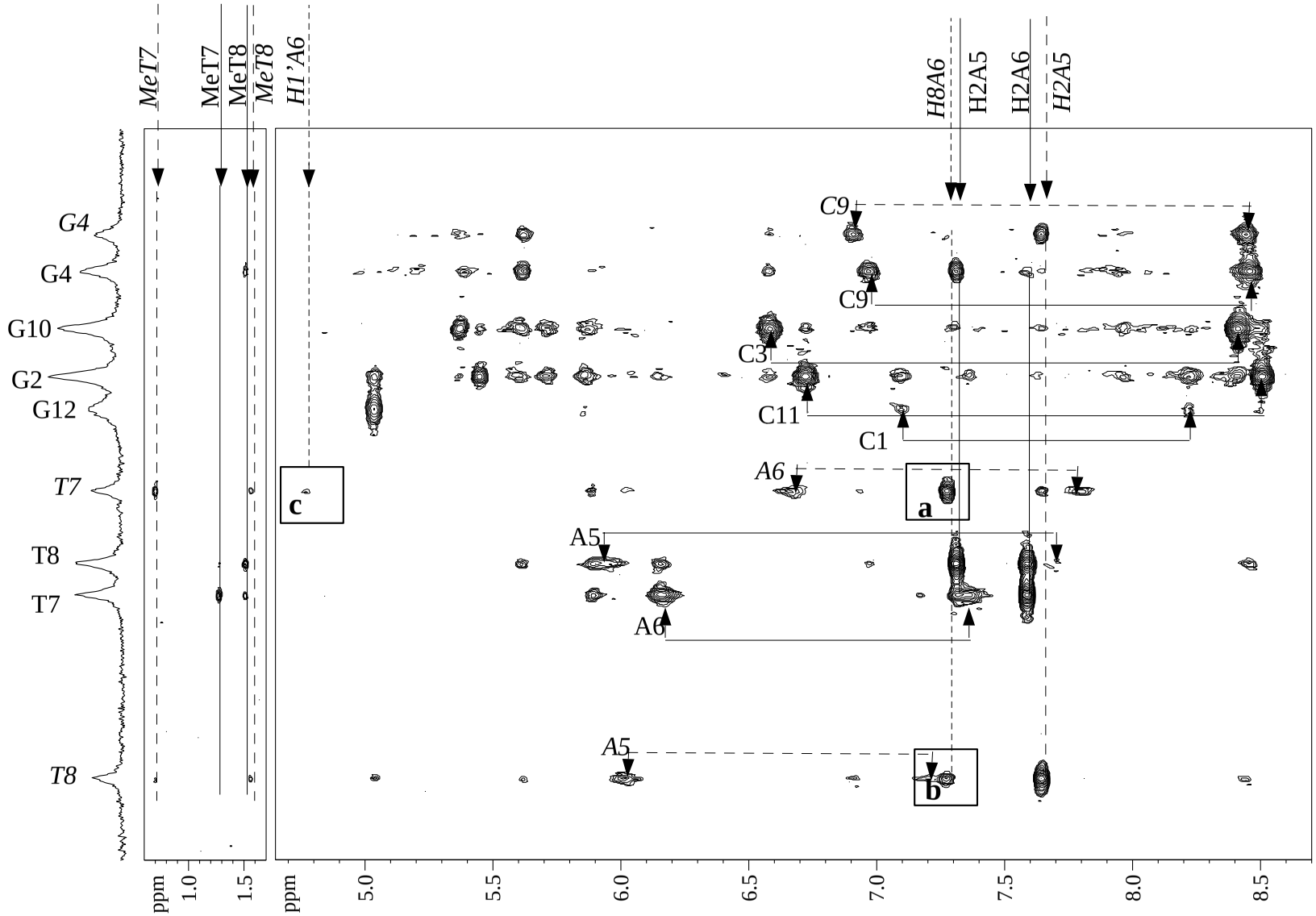
MeT7
MeT7
MeT8
MeT8
H1'A6
H8A6
H2A5
H2A6
H2A5
G4
G4
G10
G2
G12
T7
T8
T7
T8
C9
C9
C3
C11
C1
A6
A5
A6
A5
a
b
c
ppm
1.0
1.5
ppm
5.0
5.5
6.0
6.5
7.0
7.5
8.0
8.5

Figure 6

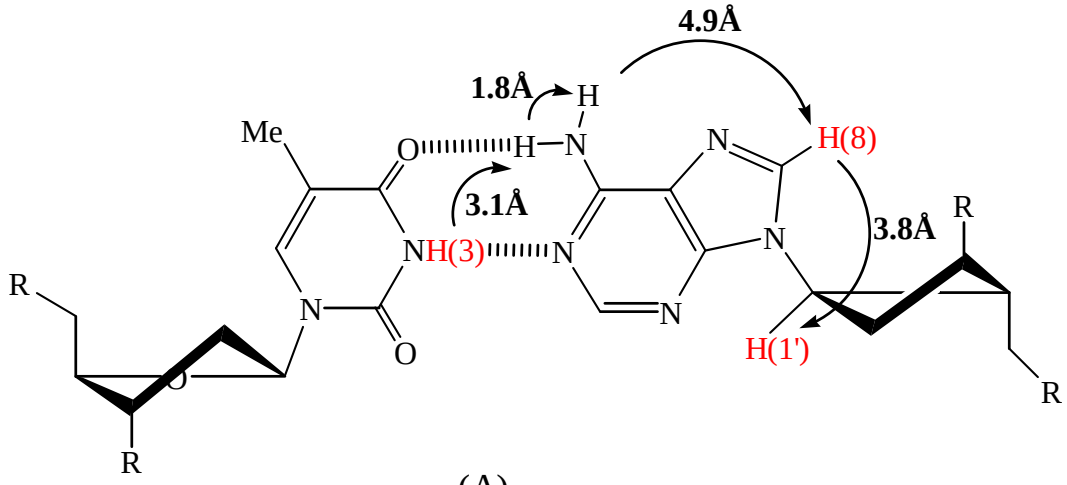
4.9Å
1.8Å
H
Me
O
H
N
N
H(8)
3.1Å
NH(3)
N
N
3.8Å
R
R
N
N
H(1')
O
O
R
R

(A)

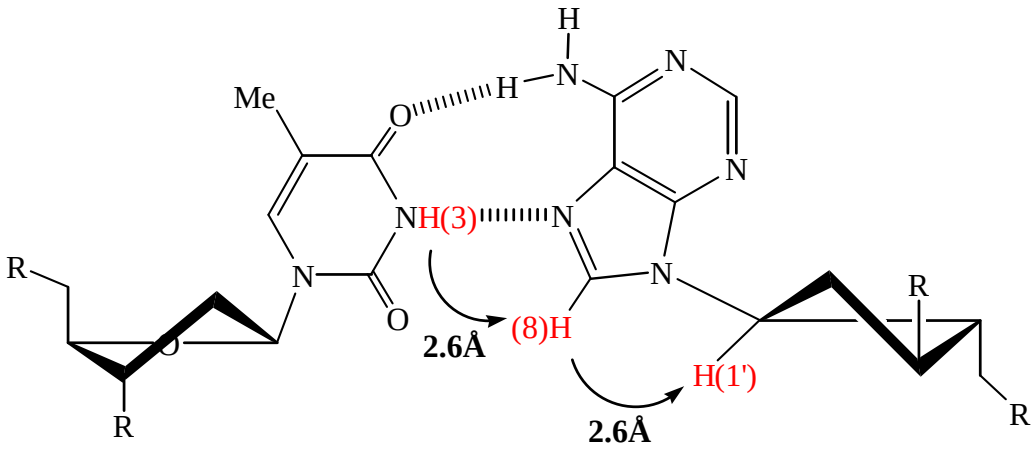
H
Me
O
H
N
N
N
NH(3)
N
N
R
N
O
2.6Å
(8)H
R
H(1')
O
R
2.6Å
R

(B)

Figure 7

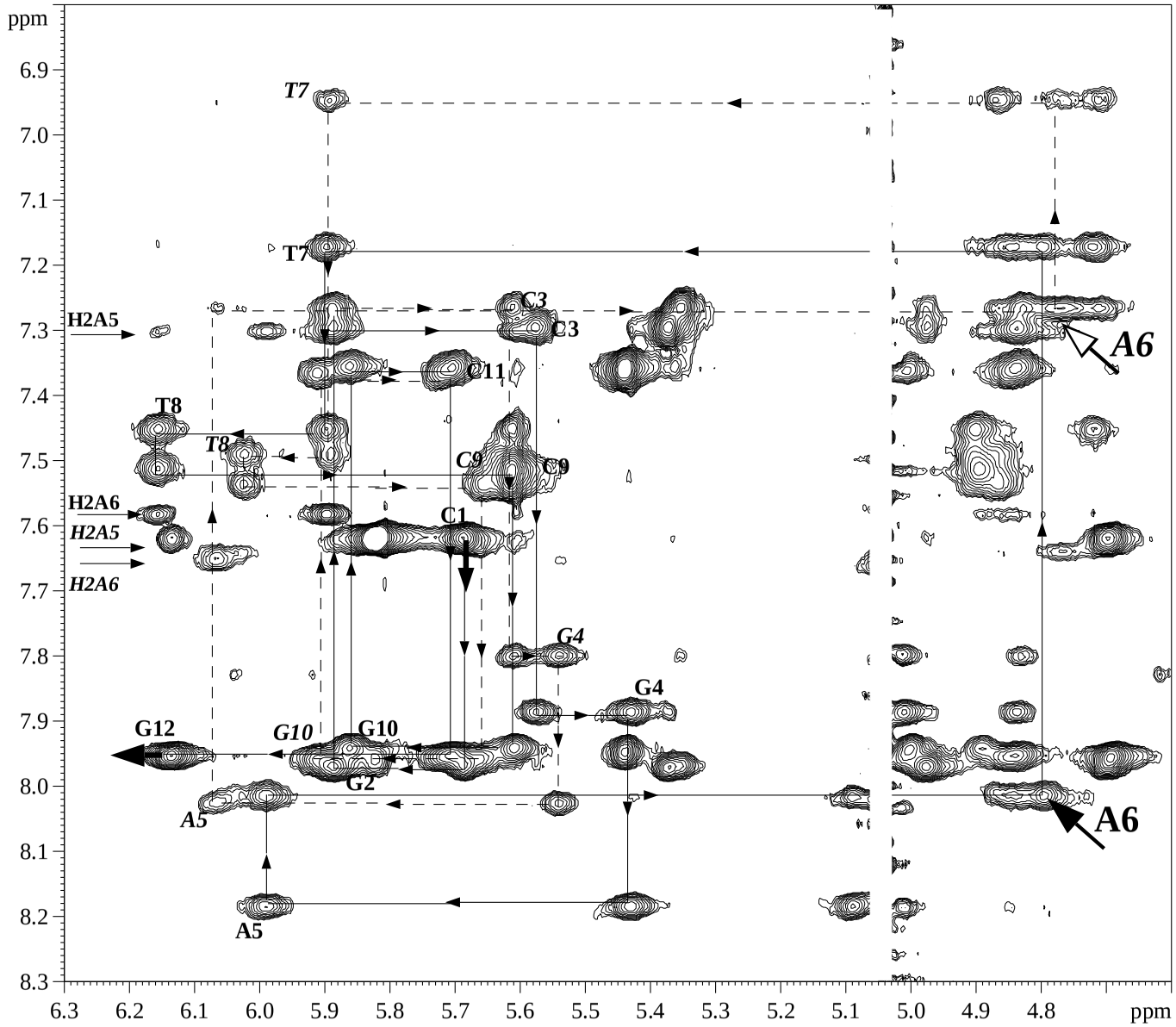
ppm
6.9
7.0
7.1
7.2
7.3
7.4
7.5
7.6
7.7
7.8
7.9
8.0
8.1
8.2
8.3
T7
T7
H2A5
C3
C3
C11
T8
T8
C9
C9
H2A6
H2A5
H2A6
C1
G4
G4
G12
G10
G10
G2
A5
A5
A6
A6
6.3
6.2
6.1
6.0
5.9
5.8
5.7
5.6
5.5
5.4
5.3
5.2
5.1
5.0
4.9
4.8
ppm

Figure 8

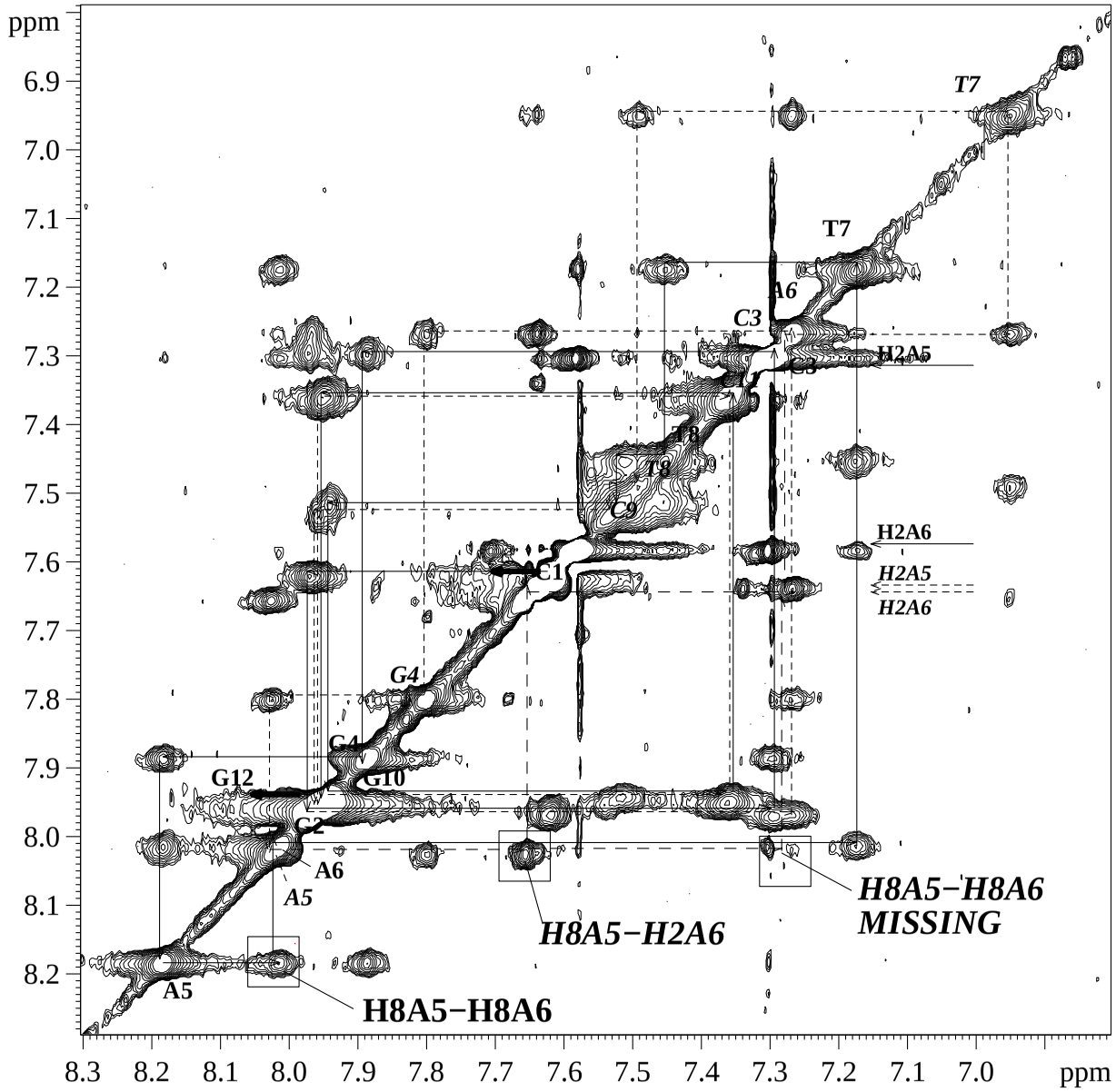
ppm
6.9
7.0
7.1
7.2
7.3
7.4
7.5
7.6
7.7
7.8
7.9
8.0
8.1
8.2
8.3
8.2
8.1
8.0
7.9
7.8
7.7
7.6
7.5
7.4
7.3
7.2
7.1
7.0
ppm
T7
T7
C3
H2A5
T8
T8
C9
H2A6
H2A5
H2A6
C1
G4
G4
G12
G10
C2
A6
A5
A5
H8A5−H2A6
H8A5−H8A6
MISSING
H8A5−H8A6

Figure 9

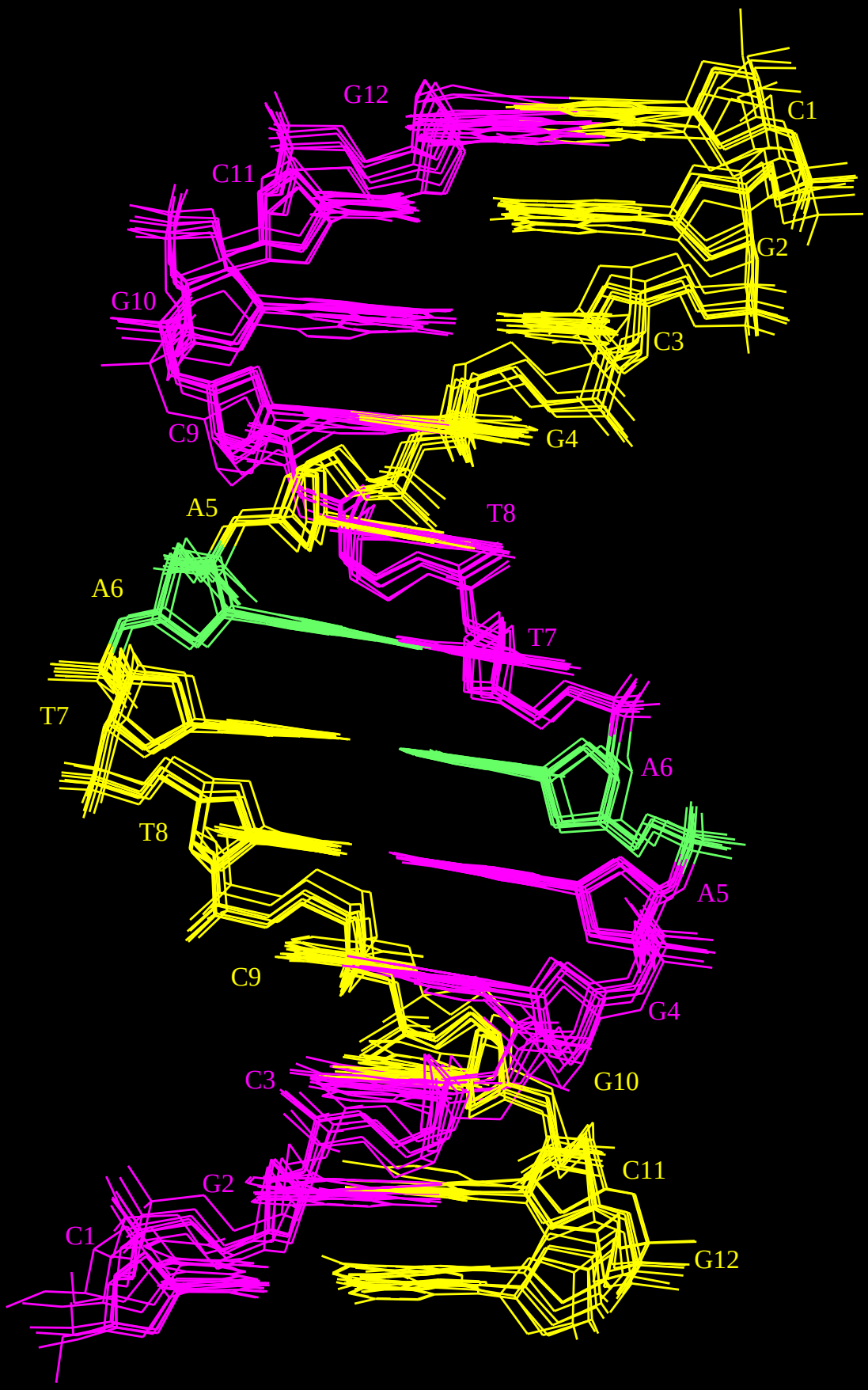
G12
C1
C11
G2
G10
C3
C9
G4
A5
T8
A6
T7
T7
A6
T8
A5
C9
G4
C3
G10
C11
G2
C1
G12

Figure 11

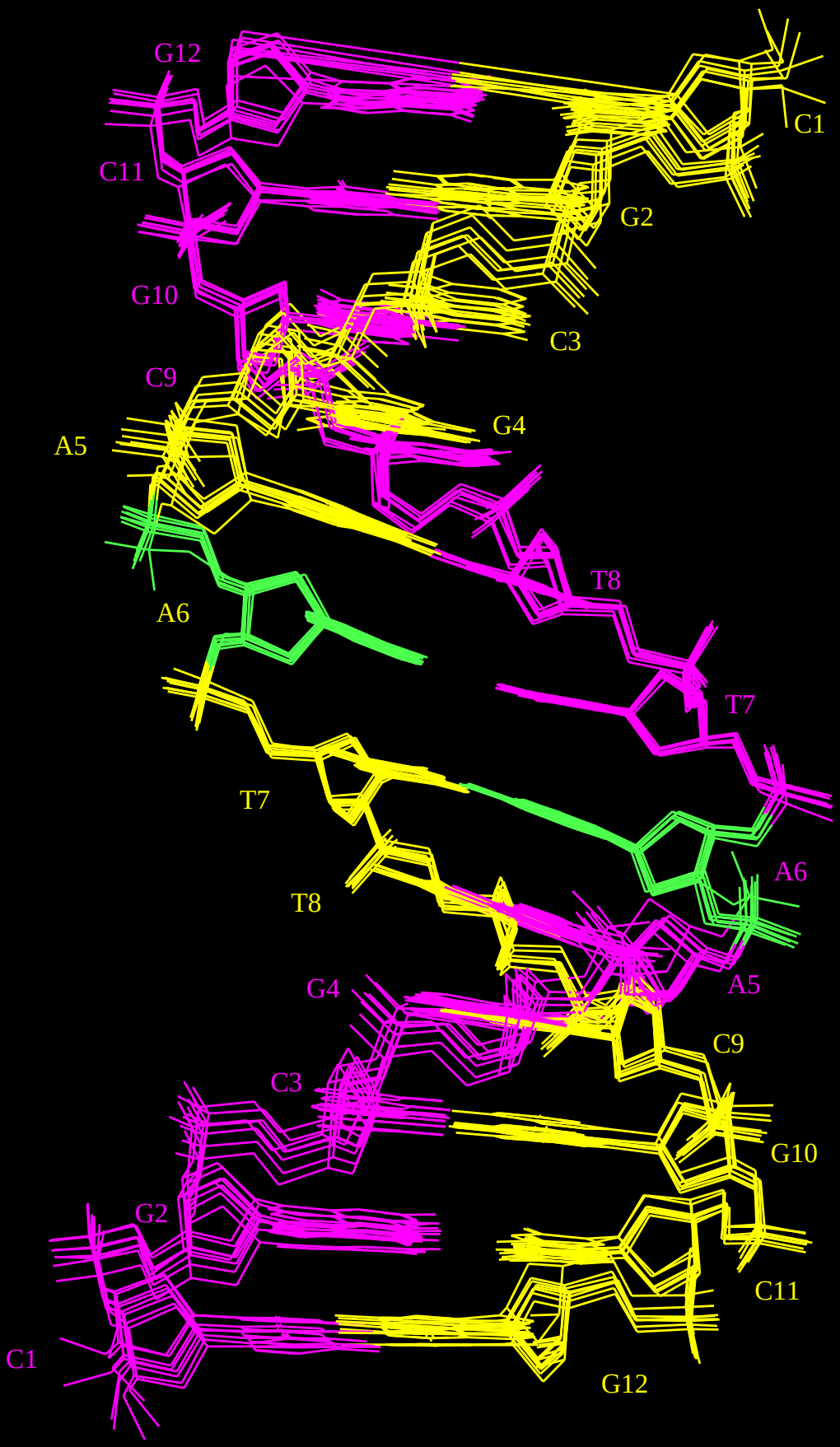
G12
C1
C11
G2
G10
C3
C9
G4
A5
T8
A6
T7
T7
A6
T8
A5
G4
C9
C3
G10
G2
C11
C1
G12

Figure 12